Available online at www.sciencedirect.com

SciVerse ScienceDirect

Geochimica et Cosmochimica Acta 94 (2012) 22–37

Geochimica et Cosmochimica Acta

www.elsevier.com/locate/gca

Sources and input mechanisms of hafnium and neodymium in surface waters of the Atlantic sector of the Southern Ocean

Torben Stichel [a,b,*], Martin Frank [a], Jörg Rickli [c], Ed C. Hathorne [a], Brian A. Haley [d], Catherine Jeandel [e], Catherine Pradoux [e]

[a] GEOMAR, Helmholtz Centre for Ocean Research Kiel, Wischhofstr. 1-3, 24148 Kiel, Germany
[b] SOEST, University of Hawaii at Manoa, 1680 East-West Rd., Honolulu, HI 96822, USA
[c] Department of Earth Sciences, University of Bristol, Wills Memorial Building, Bristol BS8 1RJ, UK
[d] COAS, Oregon State University, 104 Ocean Admin. Bldg., Corvallis, OR 97331, USA
[e] LEGOS (UMR 5566 CNRS, CNES, IRD, UPS) Observatoire Midi-Pyrénées, 14 Avenue Edouard Belin, 31400 Toulouse, France

Received 20 October 2011; accepted in revised form 9 July 2012; available online 20 July 2012

Abstract

Radiogenic isotopes of hafnium (Hf) and neodymium (Nd) are powerful tracers for water mass transport and trace metal cycling in the present and past oceans. However, due to the scarcity of available data the processes governing their distribution are not well understood. Here we present the first combined dissolved Hf and Nd isotope and concentration data from surface waters of the Atlantic sector of the Southern Ocean. The samples were collected along the Zero Meridian, in the Weddell Sea and in the Drake Passage during RV Polarstern expeditions ANTXXIV/3 and ANTXXIII/3 in the frame of the International Polar Year (IPY) and the GEOTRACES program. The general distribution of Hf and Nd concentrations in the region is similar. However, at the northernmost station located 200 km southwest of Cape Town a pronounced increase of the Nd concentration is observed, whereas the Hf concentration is minimal, suggesting much less Hf than Nd is released by the weathering of the South African Archean cratonic rocks. From the southern part of the Subtropical Front (STF) to the Polar Front (PF) Hf and Nd show the lowest concentrations (<0.12 pmol/kg and 10 pmol/kg, respectively), most probably due to the low terrigenous flux in this area and efficient scavenging of Hf and Nd by biogenic opal. In the vicinity of landmasses the dissolved Hf and Nd isotope compositions are clearly labeled by terrigenous inputs. Near South Africa Nd isotope values as low as $\varepsilon_{Nd} = -18.9$ indicate unradiogenic inputs supplied via the Agulhas Current. Further south the isotopic data show significant increases to $\varepsilon_{Hf} = 6.1$ and $\varepsilon_{Nd} = -4.0$ documenting exchange of seawater Nd and Hf with the Antarctic Peninsula. In the open Southern Ocean the Nd isotope compositions are relatively homogeneous ($\varepsilon_{Nd} \sim -8$ to -8.5) towards the STF, within the Antarctic Circumpolar Current, in the Weddell Gyre, and the Drake Passage. The Hf isotope compositions in the entire study area only show a small range between $\varepsilon_{Hf} = +6.1$ and $+2.8$ support Hf to be more readily released from young mafic rocks compared to old continental ones. The Nd isotope composition ranges from $\varepsilon_{Nd} = -18.9$ to -4.0 showing Nd isotopes to be a sensitive tracer for the provenance of weathering inputs into surface waters of the Southern Ocean.

1. INTRODUCTION

1.1. Hafnium and neodymium isotopes as tracers in seawater

Dissolved radiogenic hafnium (Hf) and neodymium (Nd) isotope compositions (expressed as ε_{Hf} and ε_{Nd} by

* Corresponding author at: SOEST, University of Hawaii at Manoa, 1680 East-West Rd., Honolulu, HI 96822, USA
E-mail address: tstichel@hawaii.edu (T. Stichel).

0016-7037/$ - see front matter © 2012 Elsevier Ltd. All rights reserved.
http://dx.doi.org/10.1016/j.gca.2012.07.005

normalizing the $^{176}Hf/^{177}Hf$ and the $^{143}Nd/^{144}Nd$ to that of CHUR in parts per 10,000 (Jacobsen and Wasserburg, 1980; Nowell et al., 1998)) in seawater have been shown to provide insights into present and past ocean circulation and weathering conditions on land (e.g. Piotrowski et al., 2000; Frank et al., 2002; van de Flierdt et al., 2002). The global average residence time of Nd in the ocean is between 360 and 1500 years, allowing the use of Nd isotopes as a tracer for advection and mixing of water masses over long distances (Jeandel et al., 1995; Tachikawa et al., 1999; Siddall et al., 2008; Arsouze et al., 2009; Rempfer et al., 2011). Hafnium, on the other hand, has an oceanic residence time, which is most likely on the order of only few hundred years (Rickli et al., 2009; Zimmermann et al., 2009b), implying that radiogenic Hf isotopes are useful tracers for water masses restricted to basin scales. However, there are also estimates for the residence time of Hf in the deeper ocean longer than that of Nd, whereas in the surface ocean the opposite was proposed (Godfrey et al., 2008, 2009). This discrepancy is mainly due to the lack of information available on the distribution of dissolved Hf in seawater and the isotopic range of the input sources. While the Nd input into the ocean is known to be governed by river and groundwater contributions, as well as exchange between sediments and seawater (Elderfield et al., 1990; Greaves et al., 1994; Jeandel et al., 1995; Haley et al., 2004; Lacan and Jeandel, 2005), the inputs contributing to the marine Hf budget are still debated. Hafnium in seawater is possibly delivered mainly by fluvial input (e.g. Bayon et al., 2006; Godfrey et al., 2008) but also partial dissolution of dust (Albarède et al., 1998; David et al., 2001; Pettke et al., 2002; Godfrey et al., 2009; Rickli et al., 2010), exchange with marine sediments similar to Nd (Lacan and Jeandel, 2005), and hydrothermal inputs (Bau and Koschinsky, 2006) may play a role.

Comparison of the relationship between the Hf and Nd isotopes in terrestrial rocks, referred to as the "terrestrial array" (Patchett et al., 1984; Vervoort et al., 1999), with available seawater data (Godfrey et al., 2009; Rickli et al., 2009, 2010; Zimmermann et al., 2009a,b) reveals fundamental differences (Fig. 1A). The Hf and Nd isotope composition of terrestrial rocks is governed by a very similar lutetium–hafnium (Lu/Hf) and samarium–neodymium (Sm/Nd) elemental fractionation during igneous processes. The radiogenic isotope systems of Hf and Nd are controlled by the decay of their respective parent isotopes ^{176}Lu and ^{147}Sm: Continental crustal rocks are thus characterized by low Lu/Hf and low Sm/Nd leading to unradiogenic bulk Hf and Nd isotope compositions (low ε-values) over time. Mafic rocks (i.e. mantle-derived rocks) have higher Lu/Hf and Sm/Nd and are therefore more radiogenic (higher ε-value) in their bulk Hf and Nd isotope compositions. Compared to the terrestrial array, the available seawater Hf and Nd isotope data ("seawater array") are shifted to more radiogenic Hf isotope compositions for a given Nd isotope composition. The most plausible explanation is that during incongruent weathering of continental crust, unradiogenic Hf is retained in weathering resistant minerals, such as zircons, a process often referred to as the "zircon effect" (Patchett et al., 1984; Albarède et al., 1998; Piotrowski et al., 2000; van de Flierdt et al., 2002, 2007). In addition, minerals with highly radiogenic Hf isotope composition have been shown to be more susceptible to weathering, thus causing preferential supply of radiogenic Hf to seawater (Bayon et al., 2006, 2009; van de Flierdt et al., 2007; Chen et al., 2011). Rickli et al. (2010) suggested that areas with high atmospheric dust loads, such as the Sahara region, also act as sources of Hf to seawater. Comparing the surface ocean Hf isotope compositions to those of dust indicates that Hf is preferentially released from traces of radiogenic apatite and clays resulting in a surface water Hf isotope composition, which is $\sim$10 ε_{Hf} units more radiogenic than the bulk dust composition in the Atlantic Ocean. Therefore, both fluvial and atmospheric inputs are likely to contribute to the radiogenic Hf isotope composition in the ocean. An alternative explanation, although so far not supported by direct data, is the input of radiogenic Hf through hydrothermal venting (Bau and Koschinsky, 2006; White et al., 1986). This source has been shown not to deliver any radiogenic Nd to deep waters (German et al., 1990; Halliday et al., 1992) and thus could also explain the observed offset to more radiogenic Hf isotope compositions of seawater.

Despite of the existence of Hf and Nd isotope data from different parts of the global ocean the continental contributions and their supply pathways are still largely unconstrained, in particular in the Southern Ocean. In addition, the Southern Ocean is characterized by a high biogenic opal productivity, which may play an important role for the cycling of Hf and the rare earth elements (REE). Here we present the first combined surface water Hf and Nd isotope compositions and concentrations complemented by REE distributions from the Atlantic sector of the Southern Ocean. With this new dataset we aim at better understandings of the external inputs of Hf and Nd and of the mechanisms, which control their elemental and isotopic distribution in the surface ocean. Comparison of REE patterns from surface waters with those of potential sources allow the processes governing their distribution to be evaluated.

1.2. Study area

The surface waters of the Southern Ocean (Fig. 2) are separated from those of the subtropical region further north by a pronounced meridional temperature and salinity gradient. This hydrographic boundary is referred to as the Subtropical Front (STF, Hofmann, 1985). The STF is the only front in the Southern Ocean that is not circumpolar, given that no subtropical waters are found in the Drake Passage between the Antarctic Peninsula and South America (Sievers and Emery, 1978; Sievers and Nowlin, 1984). The STF marks the transition between the relatively cold and fresh Subantarctic Surface Water (SASW) and the much warmer and saltier Subtropical Surface Water (STSW). The front develops in the western South Atlantic Ocean and is associated with an eastward transport of up to 37 Sv (1 Sv = 10^6 m^3s^{-1}). This flow decreases to less than 15 Sv towards South Africa, commonly called the South Atlantic Current (SAC) where it turns north to feed the

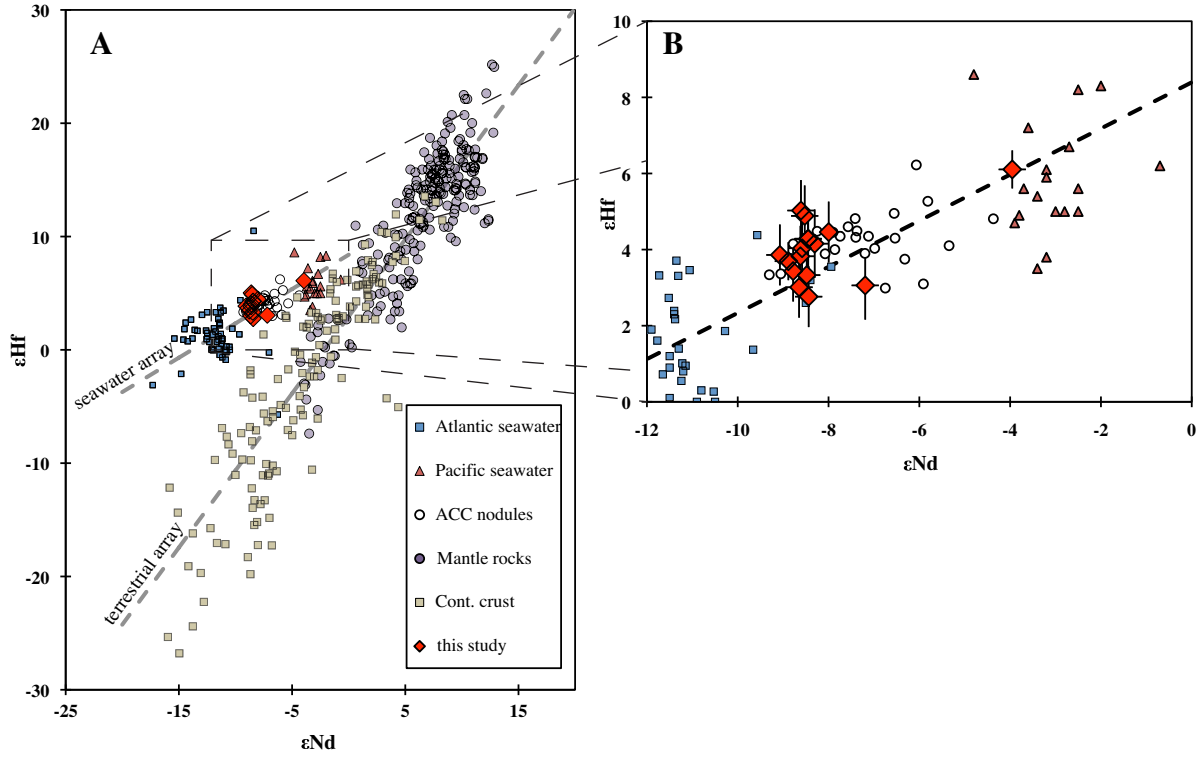

Fig. 1. Hf and Nd isotope compositions of terrestrial rocks ("terrestrial array"), seawater and ferromanganese crusts ("seawater array"). The terrestrial array (Vervoort et al., 1999) is characterized by a larger ε_{Hf} variability than that of ε_{Nd} (A). The seawater array displays more radiogenic ε_{Hf} for a given ε_{Nd} value (B). Atlantic Hf isotope compositions (Godfrey et al., 2009; Rickli et al., 2009, 2010) plot at the unradiogenic end of the array, whereas Pacific compositions (Zimmermann et al., 2009a) form the radiogenic part. The Hf and Nd isotope compositions of Southern Ocean seawater as well as of ferromanganese crusts and nodules (van de Flierdt et al., 2006) plot between Atlantic and Pacific compositions.

Benguela Current (Stramma and Peterson, 1990). South of the STF, a region of weak flow separates the SAC from the Antarctic Circumpolar Current (ACC), which dominates geostrophic eastward flow around the Antarctic continent. The ACC is bound to the south by cyclonically circulating gyres, such as the Weddell Gyre (WG, Deacon, 1979; Klatt et al., 2005). Within the ACC, bands of pronounced horizontal density gradients, also associated with strong lateral currents, characterize the Subantarctic (SAF) and the Polar (PF) Fronts (Emery, 1977; Nowlin and Whitworth, 1977; Whitworth, 1980; Peterson and Stramma, 1991). From the PF to the Antarctic continent the relatively homogenous Antarctic Surface Water (AASW) is found, which forms the topmost layer above the warmer and saltier Upper (U) and Lower (L) Circumpolar Deep Water (CDW).

The Atlantic sector of the Southern Ocean is bounded by the landmasses of South Africa in the east, the Antarctic continent in the south and South America in the west (Fig. 2). The geology of South Africa mainly comprises the Archaean Kaapvaal Craton, which is surrounded by several orogenic belts of Proterozoic and Paleozoic age. On top of this old basement the sedimentary Karoo Basin developed during the Paleozoic (Cole, 1992). The geological structure of the Antarctic continent (Fig 2A) can be broadly divided into the three tectonic domains comprising the East Antarctic Shield (EAS), the Transantarctic Mountains (TAM) and West Antarctica (WA). The EAS comprises a Precambrian to Ordovician igneous and sedimentary basement overlain by Devonian to Jurassic sediments. East Antarctica, in particular the Dronning Maud Land (DML), consists of approximately the same tectonic facies as South Africa, in both cases originating from the Pan-African orogeny which formed during the collision of East and West Gondwana about 600–500 Ma ago (Thomas et al., 1993; Rogers et al., 1994). The TAM mark the boundary between East and West Antarctica. They consist of sedimentary deposits from the Late Cambrian Ross orogeny, Devonian to Permian sediment covers of Gondwana, and Jurassic tholeiites. The TAM underwent uplift since the early Cretaceous (Dalziel, 1992; Fitzsimons, 2000). West Antarctica has five crustal blocks, of which three are relevant for this study: the Haag Nunataks (HN), the Ellsworth Whitmore Mountains (EWM) and the Antarctic Peninsula (AAP). The HN represents a small crustal block between the AAP and the EWM consisting of Proterozoic amphibolites and orthogneisses (Millar and Pankhurst, 1987). The EWM form a 415 km long, NNE–SSW trending mountain chain being a terrane once situated at the margin of Gondwana prior to its break-up during the Jurassic (Dalziel, 1992; Storey, 2005). The AAP mainly consists of magmatic rocks of varying origin and is interpreted as a

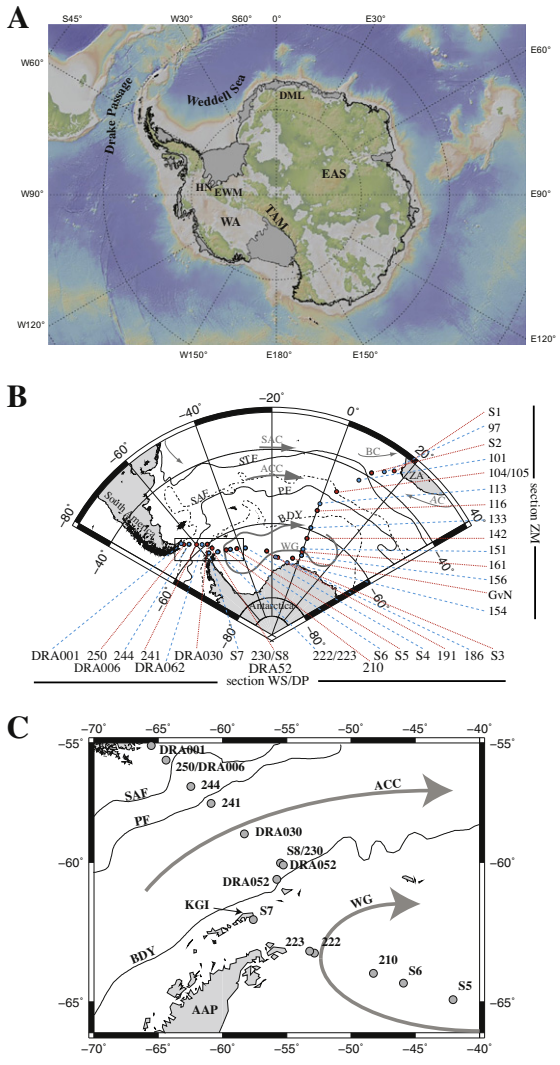

Fig. 2. Overview of the study area. The upper map (A) shows the bedrock configuration of Antarctica together with the major shelf ice contours (grey areas). The main geologic terrains are displayed: Antarctic Peninsular (AAP), East Antarctic Shield (EAS), Ellsworth Whitmore Mountains (EWM), Dronning Maud Land (DML), Haag Nunataks (HN), Transantarctic Mountains (TAM) and West Antarctica (WA). The map was constructed using GeoMapApp© (http://www.geomapapp.org) with the topography after Ryan et al. (2009). (B) Shows the sample sites and the hydrographic surface conditions and (C) is an enlargement of the area near the Antarctic Peninsula and King George Island (KGI). The main hydrographic features are the Agulhas Current (AC), the Antarctic Circumpolar Current (ACC), the Benguela Current (BC), the South Atlantic Current (SAC) and the Weddell Gyre (WG). The dashed and dotted lines in (B) and (C) represent the approximate locations of the Southern Ocean frontal system from north to south: the Subtropical Front (STF, the Subantarctic Front (SAF), the Polar Front (PF) and the Southern ACC boundary (BDY) as described in Orsi et al. (1995).

long-lived magmatic arc partly built on Cambrian continental crust (Millar et al., 2001). Most of the exposed rocks, however, are of Mesozoic and younger ages resulting from subduction on the western margin of the Peninsula. These consist of the AAP Batholith, which reflects central arc magmatism, and back-arc sequences on the eastern side of the Peninsula bounded by the Weddell Sea. Across the Drake Passage to the north these back-arc sequences continue as the southern part of South America (Patagonia). Together with the AAP, Patagonia forms one of the largest igneous provinces on Earth (Pankhurst et al., 1998).

2. METHODS

2.1. Sample collection and onboard procedures

Most samples were collected during the International Polar Year (IPY) cruise ANTXXIV/3 on the German research vessel *FS Polarstern* from February to April 2008. This cruise was also part of the international GEOTRACES program and all samples were collected and measured for their Nd and Hf concentrations and isotope compositions according to the agreed GEOTRACES protocols (http://www.obs-vlfr.fr/GEOTRACES/libraries/documents/Intercalibration/Cookbook.pdf). Between 100 and 130 L of seawater were taken for each sample mostly when the ship was underway. The collection was carried out in three different ways: (1) using a towed stainless steel fish with a Teflon head, through which surface water was pumped directly into the ship's laboratory under trace metal clean conditions, (2) using the ship's own seawater intake system made of polypropylene tubes, or (3) using Niskin bottles on a CTD rosette collecting water from 25 to 480 m water depth during station time (Table 1 and Fig. 2). For this study we refer to samples shallower than 100 m as *surface samples*. All samples were filtered through a 142 mm MilliPore® filter disc with a pore size of 0.45 μm into acid cleaned LDPE cubitainers. Filtration was performed within 12 h after collection or directly during collection when possible. The samples were then acidified to pH ~2 with double distilled, concentrated HNO_3. From each sample an aliquot of 2 L was kept for concentration analysis. About 500–600 mg iron (Fe), in the form of previously cleaned dissolved Fe–chloride, was added to the large volume samples and left for 24 h for equilibration. In a second step, ammonia solution (25%, Merck Suprapur®) was added to bring the pH back to 8 in order to co-precipitate the dissolved trace metals (i.e. Hf and Nd) with Fe hydroxide (FeOOH). The supernatant was discarded and the residual FeOOH precipitate was transferred into pre-cleaned 2 L LDPE-bottles.

In addition, five Nd samples collected in the Drake Passage during the expedition ANTXXIII/3 on *Polarstern* were included in this study (see Table 1). For each of these samples 10 L of seawater were filtered and acidified as described above. The pre-concentration was realized by co-precipitation with manganese hydroxide (MnOOH) after increasing the pH to ~8. The MnOOH precipitate was filtered on board in a laminar flow hood and the filters were stored away for further analysis on shore.

2.2. Further procedures in the home laboratory

The FeOOH precipitates obtained during ANTXXIV/3 were centrifuged in the home laboratory of GEOMAR in Kiel (Germany) and were rinsed at least twice with de-

ionized water (MilliQ, 18.2 MΩcm) to wash out major ions. The precipitate was removed from the centrifuge tubes and transferred into 60 ml Teflon vials with 5 ml 6 M HCl (quartz distilled). After evaporation, 4 ml of aqua regia were added and the closed vials were heated at 110 °C for at least 24 h to destroy organic compounds. The samples were then transformed to Cl-form and finally dissolved in 4 ml of 6 M HCl. The majority (more than 99%) of the Fe was removed prior to chromatographic separation by solvent extraction with di-ethyl ether (Stichel et al., 2012). The residual was then evaporated and re-dissolved in 4 ml 3 M HCl.

Most of the samples formed a jelly-like silica gel in HCl, which scavenged about 90% of the Hf from the sample. This silica gel was isolated and dissolved with 2 M HF. After evaporation of the 2 M HF, this fraction was recombined with the HCl soluble fraction of the same sample. The purification of Hf and separation of REE followed a modified recipe of Münker et al. (2001). Some remaining traces of ytterbium (Yb), which would have caused an isobaric interference on ^{176}Hf, were subsequently removed on an additional column loaded with 1.4 ml of cation-exchange resin (Biorad® AG50W-X8, 200–400 μm mesh-size) using 1 M HCl and 0.05 M HF to elute Hf before the rare earth elements (REE). Purification after Münker et al. (2001) also allowed the separation of the REE from most of the sample matrix. The REE were eluted in 6 M HCl immediately after loading the sample. The REE cut was further processed using LN-Spec resin following Pin and Zalduegui (1997). The respective Hf and Nd cuts were treated with 100 μl HNO_3 (concentrated, quartz distilled) and 100 μl H_2O_2 (30 wt.%, Merck Suprapur®) in preparation for mass spectrometry to avoid potentially disturbing matrix effects by traces of resin or other residual organic compounds. Finally the samples were dissolved in 0.5 M HNO_3 (Nd) and 0.5 M HNO_3 + 0.1 M HF (Hf) for measurement on the MC-ICPMS.

The filtered MnOOH precipitates from the additional samples from expedition ANTXXIII/3 were dissolved and further treated at *LEGOS* in Toulouse (France). Extraction of the "REE fraction" from the MnOOH co-precipitate was conducted on an anion exchange resin following the procedure described in Jeandel et al. (2011). Neodymium was then purified following the two-step procedure of Lacan and Jeandel (2001).

2.3. Concentration measurements

Hafnium and neodymium concentrations were obtained by isotope dilution (ID) similar to the method described by Rickli et al. (2009). For the five additional samples, only Nd concentrations were determined following Lacan and Jeandel (2001). Weighed spike solutions of ^{178}Hf and a mixture of ^{150}Nd/^{149}Sm were added to an acidified 0.5 L aliquot of each sample. The samples were left for 4–5 days to completely equilibrate. Subsequently $FeCl_3$ was added to the samples and Hf and Nd were co-precipitated with FeOOH by adding ammonia to raise the pH to 8. For mass spectrometric analysis, purification of Hf and Nd using a single cation chromatographic separation step (1.4 ml resin bed, Biorad® AG50W-X8, 200–400 μm mesh-size) was sufficient. Hafnium was loaded and collected in a mixture of 1 M HCl and 0.05 M HF (0.5 ml loading solution, 2 additional ml for elution), whereas Nd was collected in 5 ml 6 M HNO_3, following the elution of barium in 12 ml of 2 M HNO_3. The respective cuts containing Nd and Hf were evaporated to dryness and then oxidized by adding 200 μl of a 1:1 mixture of 0.5 M HNO_3 and H_2O_2 (30 wt.%) to destroy remaining organic compounds originating from the resin before measurement on the MC-ICPMS. Replicates for each element were processed and yielded an external reproducibility of better than 1% for Nd and between 3% and 10% for Hf depending on concentration. Laboratory blanks were quantified by processing 0.5 L of MQ-water in the same way as the samples and corresponded to less than 1% for Nd, where no blank corrections were applied. The Hf content of the samples being very low was closer to the blank level. The blank amounted to 5 ± 0.7 pg ($n = 11$, corresponding to 50% of the smallest sample), which was subtracted from all samples to achieve a correct seawater concentration.

The concentrations of all the naturally occurring rare earth elements (REE) concentrations were determined using a seaFAST system (Elemental Scientific Inc.) connected to an *Agilent* 7500ce ICP-MS. The seaFAST system performs preconcentration, matrix removal and online elution into the ICP-MS enabling direct analysis of trace metals from 4 ml of undiluted seawater (Hathorne et al., 2012). The overall reproducibility for all REE concentrations was better than 8% (1 SD), estimated from repeated measurements of a seawater sample ($n = 10$). The agreement for Nd concentrations between the seaFast measurements and isotope dilution is better than 10% for most of the samples except for stations S3, S7 and 222 (180 m), where the seaFAST produced 13.7%, 13.0% and 15.3% higher concentrations.

2.4. Isotope measurements

The Hf isotope compositions were measured on a Nu Plasma HR MC-ICPMS at GEOMAR applying manual time resolved data acquisition. The samples were dissolved in 250–500 μl 0.5 M HNO_3/0.1 M HF to obtain a Hf concentration of ~20 ppb corresponding to a total beam of at least 4 V. The measured Hf isotope ratios were integrated over the time of analysis (3–5 min) and corrected for instrumental mass fraction to ^{179}Hf/^{177}Hf = 0.7325 applying an exponential mass fractionation law. All ^{176}Hf/^{177}Hf ratios were normalized to the accepted value for JMC 475 of 0.28216 (Nowell et al., 1998) using the average of repeated measurements of the JMC 475 standard in each session. The external reproducibility for the set of samples in this study was ±0.8 ε_{Hf} (2 SD) and was estimated by 4–6 repeated measurements of the JMC 475 Hf standard during every session at the same concentration as the samples. The Nd isotope composition was either also measured on the *Nu plasma* instrument, though in automatic mode, or on a Thermo Scientific Triton1 TIMS. The measured isotopic composition was corrected for instrumental mass bias to ^{146}Nd/^{144}Nd = 0.7219 applying an exponential mass fractionation law. All ^{143}Nd/^{144}Nd ratios were normalized to

the JNdi-1 standard with the accepted ratio of 0.512115 (Tanaka et al., 2000) using the average of the repeatedly measured standard of the respective session. The external reproducibility was between ±0.3 ε_{Nd} and ±0.39 ε_{Nd} (2 SD) estimated by repeated measurements of the JNdi-1 standard, as well as of an internal laboratory standard. Duplicates measured on both instruments resulted in the same value within this error. The blanks for both elements (laboratory work only) were ~20 pg (Hf) and ~50 pg (Nd), which in both cases was less than 1% of the smallest sample.

The additional samples from ANTXXIII/3 were measured on a MAT 261 TIMS (Observatoire Midi-Pyrénées, Toulouse, France), using the same method as described above to correct for instrumental mass bias. These samples were normalized to the La Jolla Nd standard with the accepted $^{143}Nd/^{144}Nd$ value of 0.511859, yielding an external reproducibility between ±0.2 and 0.6 ε_{Nd} units (2 SD). Both laboratories participated in the 2008–2010 GEOTRACES intercalibration efforts and their results agreed well within the overall 2 SD variation of ε_{Nd} ±0.6 (van de Flierdt et al., 2012).

2.5. Particles

We compared our data to results for Nd isotopes and REE concentrations in particulates from the Southern Ocean published by Hegner et al. (2007), whose study area largely overlapped with ours. Hafnium concentrations for marine particulates, which were measured on the same samples as in Hegner et al. (2007), have not been published in that study. Therefore, we analyzed these Hf concentrations for samples that were most proximal to our study sites. The methodology followed the one described in Hegner et al. (2007).

3. RESULTS

The results for dissolved Hf and REE concentrations and Hf and Nd isotope compositions from this study are presented in Tables 1 and 2. The previously published particulate Nd concentrations (Hegner et al., 2007) and the new particulate Hf concentrations are listed together in Table 3. This table also shows those stations of ANTXXIV/3 closest to those of Hegner et al. (2007).

3.1. Hf and Nd concentrations in the dissolved fraction

Both Hf and Nd concentrations show similar distribution patterns in the studied area (Fig. 3) with some distinct exceptions as will be detailed below. The Zero Median section displays the following elemental distributions from north to south (Fig. 3A): the highest Nd concentration of 24.2 pmol/kg is observed at station S1, about 200 km southwest of Cape Town. This high Nd concentration is in marked contrast to the very low Hf concentration at this station with only 0.06 pmol/kg (Table 1). The Nd concentration decreases southward to a minimum value 6.7 pmol/kg at the STF (station S2). Towards the SAF, the concentrations for both elements remain at a low level corresponding to ~6 pmol/kg for Nd and ~0.05 pmol/kg for Hf, respectively. A pronounced southward increase in the concentrations of both elements is observed between the SAF (station 104/105) and the BDY (station 113 and 116). From there onwards, the Hf and Nd concentrations remain relatively constant across the Weddell Gyre (WG) yielding typical concentrations of ~0.2 pmol/kg for Hf and ~15 pmol/kg for Nd.

The elemental distribution in the section through the Weddell Sea (east to west) and the Drake Passage (south to north) is characterized (Fig. 3B) by Hf and Nd concentrations in the Weddell Sea that are similar to those observed around the Zero Meridian in the WG. Starting approximately at station S6 the Hf concentrations, and, to a lesser extent, the Nd concentrations, rise continuously until station S7 north of the AAP. This broad maximum in concentrations with a peak value of 0.38 pmol/kg Hf and 22.6 pmol/kg Nd at station 7 occurs near King George Island. Further north in the Drake Passage Hf and Nd concentrations drop again to values similar to those found in the eastern Atlantic sector of the ACC.

3.2. REE patterns of the dissolved fraction

Fig. 4 shows PAAS-normalized (Post-Archean Average Shale, Taylor and McLennan, 1985) REE patterns for the 30 analyzed surface seawater samples (see data in Table 2). With the exception of two samples, the surface waters show shale normalized REE patterns similar to previous studies with heavy REE (HREE) enrichment compared to the light REE (LREE, e.g. Elderfield and Greaves, 1982; de Baar et al., 1983, 1985; Piepgras and Jacobsen, 1992; German et al., 1995). Stations S2 and particularly S1 show only small enrichments of the HREEs. The cerium anomalies Ce/Ce^* ($Ce/Ce^* = \log\ [3 \times Ce_N/(2 \times La_N + Nd_N)]$, whereby values <0 represent negative anomalies and REE_N is normalized to that of PAAS, Taylor and McLennan, 1985) of all samples are negative between −1.31 and −0.24 (Table 2). The smallest negative Ce anomaly was measured at station S1, close to South Africa. The most negative Ce/Ce^* values of −1.31 to −1.03 and −1.13 to −0.61 were found at stations within the Weddell Gyre and the ACC, respectively. The pronounced negative anomalies in the WG weaken close to Antarctica and only correspond to −0.56 at station 222 west of the AAP and to −0.76 at station 154 close to the DML. PAAS-normalized La–Yb ratios (La_N/Yb_N) range from 0.19 to 0.68 (Fig. 3 and Table 2). The highest La_N/Yb_N ratios were measured at S1 (0.68) and S2 (0.53). South of the STF, in the ACC and the Weddell Gyre, these ratios drop to 0.19–0.38. Like the Ce/Ce^*, the La_N/Yb_N ratios close to the AAP are similar to those in the Weddell Gyre (0.28–0.36).

3.3. Dissolved Hf and Nd isotope composition

Overall, the Hf isotope composition of the surface waters is relatively constant and most samples are between $\varepsilon_{Hf} = +2.8$ and +5.0, whereas the range of Nd isotopes is almost 15 ε_{Nd} units ($\varepsilon_{Nd} = -18.9$ to −4.0, Fig. 3). It should be noted that for the stations north of the Polar Front (PF) the Hf concentration in the samples was too low for Hf

Table 1
Dissolved trace metal data from ANTXXIV/3 and ANTXXIII/3. The hydrographic data (temperature and salinity) are from the ships own PODAS system. The data in this table are also available at http://doi.pangaea.de/10.1594/PANGAEA.786906.

Station					Device	Depth (m)	Temperature (°C)	Salinity	ε_{Nd}	Error (2σ)	Nd (pmol/kg)	ε_{Hf}	Error (2σ)	Hf (pmol/kg)
S1	34° 53.15'	S	16° 40.70'	E	Fish	5	21.03	35.47	−18.9	0.3	24.2			0.06
97	36° 59.60'	S	12° 45.40	E	CTD	100	18.23	35.55	−15.9	0.4				
S2	38° 48.00'	S	11° 35.80'	E	Fish	5	17.53	34.92	−11.0	0.3	6.7			0.04
101	42° 20.60'	S	8° 59.20'	E	CTD	75	10.21	34.55	−9.7	0.4	8.6			
104	47° 39.80'	S	4° 16.20'	E	CTD	75	6.41	33.72	−7.9	0.4	8.2			
105	47° 39.00'	S	4° 16.60'	E	Fish	5	6.50	33.71	−7.9	0.3	7.4			0.08
113	52° 59.80'	S	0° 02.00'	E	CTD	75	1.22	33.79	−7.9	0.4	16.1			
113	52° 59.80'	S	0° 02.00'	E	CTD	150	0.20	34.02	−8.0	0.4	15.0			
116	54° 21.00'	S	0° 01.00'	E	Fish	5	1.04	33.80	−8.0	0.3	15.8	4.5	0.8	0.18
133	59° 14.00'	S	0° 02.00'	E	Fish	5	0.21	33.95	−8.6	0.3	18.2			0.19
142	62° 20.00'	S	0° 00.00'	E	Fish	5	0.53	33.94	−8.6	0.3	17.3	5.0	0.8	0.11
151	65° 19.00'	S	0° 00.00'	E	Fish	5	−0.18	33.97	−8.5	0.3	17.3	4.9	0.8	0.18
154	70° 34.50'	S	8° 07.38'	W	CTD	135	−1.69	34.02	−9.9	0.4	19.4			0.22
156	67° 08.00'	S	0° 24.00'	E	Fish	5	−0.67	33.97	−8.6	0.3	19.5	3.0	0.8	0.25
161	66° 29.20'	S	0° 00.00'	E	CTD	100	0.77	34.64	−8.7	0.4	17.9			0.40
GvN	68° 31.80'	S	4° 39.00'	W	Fish	5	−1.18	33.84	−8.8	0.3	16.8	3.4	0.8	0.20
S3	69° 02.00'	S	15° 42.00'	W	Snorkel	5	–	–	−8.6	0.3	16.9	4.0	0.8	0.16
186	69° 03.00'	S	17° 25.00'	W	CTD	25	−1.84	33.93	−8.4	0.3	17.2	4.3	0.8	0.20
191	67° 21.00'	S	23° 38.00'	W	CTD	25	−1.85	34.12	−8.5	0.3	18.5	4.3	0.8	0.21
S4	65° 34.00'	S	36° 46.00'	W	Snorkel	5	−1.44	34.15	−9.0	0.3	18.5			0.18
S5	64° 59.00'	S	42° 00.00'	W	Snorkel	5	−1.55	33.91	−8.4	0.3	18.3	2.8	0.8	0.16
S6	64° 20.00'	S	46° 04.40'	W	Snorkel	5	−1.76	33.25	−8.6	0.3	18.1	3.8	0.8	0.22
210	64° 02.80'	S	48° 15.40'	W	CTD	25	−1.83	33.79	−8.5	0.3	18.3	3.3	0.8	0.27
222	63° 21.00'	S	52° 51.00'	W	CTD	25	−1.82	34.08	−8.9	0.3	19.9	3.7	0.5	0.25
222	63° 21.00'	S	52° 51.00'	W	CTD	50	−1.82	34.10	−8.9	0.4	21.2			0.29
222	63° 21.00'	S	52° 51.00'	W	CTD	100	−1.58	34.37	−8.9	0.4	19.9			0.30
222	63° 21.00'	S	52° 51.00'	W	CTD	180	−1.22	34.49	−8.7	0.4	20.4			0.32
222	63° 21.00'	S	52° 51.00'	W	CTD	280	−0.90	34.54	−8.7	0.4	21.3			0.35
222	63° 21.00'	S	52° 51.00'	W	CTD	480	−0.90	34.56	−9.1	0.3	22.5	3.9	0.8	0.34
223	63° 17.00'	S	53° 13.00'	W	CTD	25	−1.82	34.18	−8.3	0.3	21.1	4.2	0.9	0.31
S7	62° 08.00'	S	57° 31.00'	W	Snorkel	5	1.04	34.06	−4.0	0.3	22.6	6.1	0.5	0.38
S8	60° 03.00'	S	55° 24.00'	W	Snorkel	5	1.78	33.85	−7.2	0.3	14.3	3.1	0.9	0.20
230	60° 06.00'	S	55° 16.40'	W	CTD	50	0.79	34.17	−6.9	0.4	18.9			0.31
230	60° 06.00'	S	55° 16.40'	W	CTD	150	0.57	34.34	−6.4	0.4	19.9			0.35
241	57° 37.20'	S	60° 53.80'	W	CTD	50	2.84	33.79	−8.4	0.4	11.8			0.17
244	56° 53.80'	S	62° 28.00'	W	CTD	25	5.38	33.92	−8.2	0.4	10.2			0.12
244	56° 53.80'	S	62° 28.00'	W	CTD	50	5.38	33.92	−8.2	0.4	9.6			0.09
250	55° 45.50'	S	64° 26.20'	W	CTD	150	3.64	34.02	−8.2	0.4	9.7			
DRA001[a]	55° 07.00'	S	65° 33.04'	W	CTD	50	8.32	33.74	−5.7	0.6	8.5			
DRA006[a]	55° 45.00'	S	64° 30.00'	W	CTD	20	5.10	33.90	−8.6	0.3	8.9			
DRA030[a]	58° 52.00'	S	58° 18.00'	W	CTD	20	2.50	33.89	−8.2	0.5	14.7			
DRA052[a]	61° 50.00'	S	55° 26.00'	W	CTD	31	–		−6.3	0.3	21.4			
DRA062[a]	60° 39.00'	S	55° 47.00'	W	CTD	20	0.62	34.33	−7.2	0.4	17.7			

[a]Samples from ANTXXIII/3 (see text).

isotope measurements. For Nd, stations north of the STF close to South Africa have the least radiogenic Nd isotope compositions between $\varepsilon_{Nd} = -18.9$ and -11.0 (Fig. 3A). Another distinctly unradiogenic Nd isotope value of $\varepsilon_{Nd} = -9.9$ is observed in the WG at the southernmost station 154 close to the Antarctic continent. The unique deviation from the above range of Hf isotope compositions is observed at station S7, where the most radiogenic value of $\varepsilon_{Hf} = +6.1$ occurs close to King George Island (KGI, Figs. 2 and 3B). At the same station a similar excursion to more radiogenic values is also observed for Nd isotopes ($\varepsilon_{Nd} = -4.0$). At the nearby stations DRA 052, 062 and S8 north of King George Island, Nd isotope compositions between $\varepsilon_{Nd} = -6.3$ to -7.2 were measured. The Hf isotope compositions on nearby stations, on the other hand, are not elevated. A further radiogenic Nd isotope excursion in the ACC to $\varepsilon_{Nd} = -5.7$ is measured at station DRA001, close to the southern tip of Chile. Apart from these deviations the Nd isotope compositions, similar to Hf, are rather uniform within the ACC and the WG at values between $\varepsilon_{Nd} = -7.8$ and -8.6.

Combined Hf and Nd isotope compositions show that surface waters from the Southern Ocean are shifted towards more radiogenic Hf values for given Nd values when

Table 2
Dissolved REE concentration in pmol/kg, together with PAAS-normalized La/Yb ratios and Ce-anomalies (Ce/Ce^*). The REE concentrations were measured with a seaFAST system (see Section 2.3). For comparison the Nd concentration in pmol/kg obtained by isotope dilution is also provided. The data in this table are also available at http://doi.pangaea.de/10.1594/PANGAEA.786906.

Station	Depth (m)				La	Ce	Pr	Nd	Sm	Eu	Gd	Tb	Dy	Ho	Er	Tm	Yb	Lu	La/Yb (norm)	Ce/Ce*	Nd (ID)
SAC & ACC on Zero Meridian:																					
S1	5	34° 53.15' S	16° 40.7'	E	29.5	35.3	6.02	25.1	4.68	1.24	5.54	0.75	4.97	1.11	3.64	0.46	2.57	0.43	0.68	−0.24	24.2
S2	5	38° 48.00' S	11° 35.8'	E	12.1	6.47	1.52	6.77	1.53	0.29	2.00	0.29	2.25	0.71	2.03	0.24	1.43	0.17	0.50	−0.53	6.68
101	75	42° 20.60' S	8° 59.20'	E	12.3	5.90	2.05	8.99	2.14	0.34	2.49	0.43	3.00	0.94	3.18	0.37	2.52	0.45	0.29	−0.61	8.56
104	75	47° 39.80' S	4° 16.20'	E	14.1	3.53	1.95	8.61	1.82	0.49	2.60	0.45	3.63	1.05	3.74	0.55	3.54	0.70	0.24	−0.87	8.16
105	5	47° 39.00' S	4° 16.60'	E	11.9	2.60	1.54	7.21	1.41	0.42	1.99	0.42	3.83	1.12	3.81	0.51	3.73	0.64	0.19	−0.93	7.38
113	70	52° 59.80' S	0° 02.00'	E	23.6	5.64	3.34	15.1	2.80	0.87	4.59	0.74	5.73	1.47	5.37	0.81	5.26	0.97	0.27	−0.90	16.1
116	5	54° 21.00' S	0° 01.00'	E	24.5	8.34	3.69	16.6	2.77	0.76	4.68	0.64	5.71	1.49	5.16	0.90	5.39	0.94	0.27	−0.75	15.8
Weddell Gyre:																					
133	5	59° 14.00' S	0° 02.00'	E	31.9	3.74	4.50	19.8	3.60	0.93	4.86	0.85	6.22	1.63	5.91	0.88	6.01	1.05	0.31	−1.20	18.2
142	5	62° 20.00' S	0° 00.00'	E	30.3	3.60	4.08	18.3	3.41	0.86	4.61	0.76	5.95	1.73	5.64	0.88	6.02	1.04	0.30	−1.20	17.3
151	5	65° 19.00' S	0° 00.00'	E	28.7	3.63	3.94	18.0	3.19	0.83	4.50	0.70	5.94	1.57	5.77	0.80	5.62	1.15	0.30	−1.17	17.3
154	135	70° 34.50' S	8° 07.38'	W	33.9	11.0	4.95	20.9	3.46	0.91	5.08	0.88	6.02	1.65	5.97	0.97	6.71	1.14	0.30	−0.76	19.4
156	5	67° 08.00' S	0° 24.00'	E	28.4	3.75	4.03	19.5	2.95	0.80	5.00	0.71	6.05	1.62	5.80	0.84	5.45	1.01	0.31	−1.16	19.5
161	100	66° 29.20' S	0° 00.00'	E	31.1	4.53	4.40	18.6	3.19	1.02	4.67	0.81	6.24	1.72	6.43	0.89	6.50	1.23	0.28	−1.11	17.9
GvN	5	68° 31.80' S	4° 39.00'	W	29.5	3.37	4.01	16.8	3.04	0.71	6.06	0.70	6.10	1.58	5.37	0.91	5.09	1.05	0.34	−1.21	16.8
S3	5	69° 02.00' S	15° 42.00'	W	30.6	4.72	4.25	19.2	3.14	0.84	5.01	0.77	6.28	1.57	5.84	0.94	5.98	1.00	0.30	−1.09	16.9
186	25	69° 03.00' S	17° 25.00'	W	29.9	4.14	4.11	19.0	3.06	0.88	5.10	0.71	5.44	1.65	6.02	0.84	5.86	0.97	0.30	−1.13	17.2
191	25	67° 21.00' S	23° 38.00'	W	32.1	4.01	4.43	18.9	3.70	0.90	5.72	0.84	6.23	1.72	6.00	0.96	4.96	1.09	0.38	−1.17	18.5
S4	5	65° 34.00' S	36° 46.00'	W	32.6	2.92	4.36	18.7	3.48	0.87	5.05	0.80	5.97	1.77	6.03	0.92	6.06	1.10	0.32	−1.31	18.5
S5	5	64° 59.00' S	42° 00.00'	W	31.0	3.43	4.48	20.2	3.73	0.96	5.65	0.74	6.55	1.88	6.11	0.83	5.98	1.05	0.31	−1.23	18.3
S6	5	64° 20.00' S	46° 04.40'	W	30.9	3.48	4.30	19.2	3.43	0.84	5.66	0.83	5.75	1.66	5.91	0.84	6.21	1.06	0.29	−1.22	18.1
210	25	64° 02.80' S	48° 15.40'	W	30.9	5.45	4.75	20.0	3.69	0.84	4.55	0.78	5.95	1.80	5.71	0.92	6.26	1.13	0.29	−1.03	18.3
AAP & Drake passage:																					
222	50	63° 21.00' S	52° 51.00'	W	39.1	19.3	5.41	21.0	3.73	0.98	5.27	0.75	6.43	1.74	6.29	0.90	6.52	1.14	0.36	−0.56	21.2
222	180	63° 21.00' S	52° 51.00'	W	34.2	9.49	4.96	23.6	4.03	0.92	4.95	0.87	6.22	1.80	6.22	0.92	6.37	1.18	0.32	−0.84	20.4
222	280	63° 21.00' S	52° 51.00'	W	36.1	14.1	5.19	22.1	4.11	1.05	5.89	0.94	6.97	1.83	6.72	0.99	6.61	1.18	0.32	−0.68	21.3
222	480	63° 21.00' S	52° 51.00'	W	37.4	10.1	5.58	23.2	4.49	0.95	5.72	0.95	7.16	1.90	6.54	0.99	7.10	1.29	0.31	−0.84	22.5
S7	5	62° 08.00' S	57° 31.00'	W	33.6	16.2	5.80	25.6	4.98	1.19	6.49	0.96	7.24	1.99	6.60	1.08	7.22	1.29	0.28	−0.61	22.6
S8	5	60° 03.00' S	55° 24.00'	W	26.3	4.70	3.44	15.6	2.74	0.78	3.90	0.69	5.00	1.47	5.04	0.74	4.41	0.82	0.35	−1.02	14.3
230	50	60° 06.00' S	55° 16.40'	W	30.0	9.18	4.55	20.8	3.85	1.09	4.99	0.78	6.39	1.75	6.05	0.88	5.96	1.17	0.30	−0.80	18.9
230	150	60° 06.00' S	55° 16.40'	W	31.8	9.46	4.58	21.0	3.81	1.11	5.56	0.98	6.59	1.93	6.55	1.02	6.77	1.22	0.28	−0.81	19.9
241	50	57° 37.20' S	60° 53.80'	W	20.1	3.75	2.95	12.4	2.21	0.63	3.44	0.60	4.68	1.41	4.80	0.70	4.39	0.82	0.27	−1.00	11.8
244	25	56° 53.80' S	62° 28.00'	W	14.7	2.06	2.09	9.5	1.69	0.46	2.94	0.46	3.73	1.21	3.98	0.64	3.79	0.70	0.23	−1.13	10.2
244	50	56° 53.80' S	62° 28.00'	W	16.3	2.78	2.23	9.47	1.69	0.40	3.08	0.52	3.97	1.19	3.98	0.66	4.21	0.72	0.23	−1.03	9.57

compared to the "terrestrial array" (Fig. 1B). Similar to previously published seawater data (Godfrey et al., 2009; Rickli et al., 2009, 2010; Zimmermann et al., 2009a,b), the surface waters in this study plot on the "seawater array", as previously also derived from analyses of ferromanganese crust and nodule surfaces (Albarède et al., 1998; David et al., 2001; van de Flierdt et al., 2006). All samples form an isotopically tightly constrained field, with the only exception of the samples collected in the vicinity of KGI, which plot on the more radiogenic part of the seawater array.

4. DISCUSSION

4.1. Weathering inputs of Hf and REEs

4.1.1. South Africa

While the general distribution of Hf and REE concentrations, as well as Hf and Nd isotopes are similar in most parts of the study area, the data are distinctly different close to South Africa. At station S1 the Nd concentration of 24.2 pmol/kg is the highest measured in this study, whereas Hf is at its lowest level (0.06 pmol/kg). The high Nd concentration together with the shale-normalized La_N/Yb_N of 0.68 and an only slightly negative Ce anomaly ($Ce/Ce^* = -0.24$) suggest enhanced terrigenous inputs from the South African continent. A shale-normalized REE pattern comparable to that of particulate data (Hegner et al., 2007) further supports increased contributions to the dissolved REEs originating from terrigenous material, probably via partial dissolution of particles (Fig. 4). A continental input is also indicated by the very negative seawater Nd isotope composition of $\varepsilon_{Nd} = -18.9$ at S1. However, the isotope composition of suspended particles yielding ε_{Nd} of −14.5 (Hegner et al., 2007) is too radiogenic to explain the low seawater Nd isotope composition at S1. Surface sediments deposited around the South African coast are on average also more radiogenic ($\varepsilon_{Nd} = -14$ to −12, Franzese et al., 2006). Therefore, an additional source supplying unradiogenic Nd is necessary to explain the

Table 3
Particulate Hf, Nd and biogenic opal data from Hegner et al. (2007) closest to the sample sites of this study.

Sample[a]	LAT[a] (degrees N)	LON[a] (degrees E)	Biogen. SiO_2[a] (%)	Particulate Nd[a] (pmol/l)	Error (%)	Particulate Hf[b] (pmol/l)	Error (%)	Nd/Hf particles	Closest station to ANTXXIV/3[c]
z137	−39.53	18.84		0.460	4.2	0.015	13.7	30.9	S2
z01	−49.75	5.87	29	1.145	3.5	0.080	7.1	14.2	105
z02	−53.47	9.00	42	0.405	4.4	0.039	6.4	10.4	116
z04	−60.58	3.00	17	4.635	1.8				133
z05	−63.63	−0.31	8	4.028	2.6	0.148	5.9	27.2	142/151
z06	−67.27	−3.93	9	1.170	3.3	0.056	9.3	21.1	156/GvN
z71 (2)	−68.40	−26.14	58	0.231	12.3	0.042	14.2	5.4	191
z72	−66.81	−32.00	47	0.156	12.0				S4
z75	−63.03	−44.17	37	0.675	3.1	0.092	5.4	7.3	S5/S6
z76	−61.86	−52.42	27	0.076	6.0	0.009	7.5	8.5	210
z77	−62.23	−55.47		0.100	7.0	0.010	7.7	9.7	222/223
z84	−62.30	−58.65		24.438	3.1	2.882	3.7	8.5	S7
z87	−59.81	−59.69	42	0.195	3.8	0.027	14.2	7.2	S8
z89	−56.68	−63.21	29	0.142	3.6	0.010	6.7	14.8	244

[a]From Hegner et al. (2007).
[b]From the same samples of Hegner et al. (2007).
[c]This study.

unradiogenic value at S1, most plausibly surface waters advected by the Agulhas Current. The Agulhas waters may have been influenced by particle dissolution close to the eastern coast of South Africa and carry unradiogenic Nd into the Atlantic, which is supported by the provenance of deposited detritus in the southern Cape Basin (Rutberg et al., 2005; Franzese et al., 2006). Unfortunately, there are no further data available on the marine particle composition from the Indian Ocean side of South Africa to support this assumption. As mentioned above, the Hf concentration at S1 is one of the lowest of the entire sample set, which does not support an additional input from particle dissolution for Hf in that area. Thus, a release of Hf from particles appears to be of no importance or Hf is simply scavenged more readily. Unfortunately the lack of a Hf isotope value at this station does not allow to investigate if boundary exchange has been involved instead, through which the radiogenic isotope signature can change but not necessarily the concentration (e.g. Lacan and Jeandel, 2005). Possibly, Hf is largely retained in refractory minerals, such as zircon, which make it less available during particle dissolution. If Hf scavenging was high at S1, the effect on the REEs seems to be very low given the high concentration of these elements. Even though recent studies have shown that Hf is scavenged in surface waters more readily than e.g. Nd, the overall scavenging behavior of these two elements is similar (Godfrey et al., 2009; Rickli et al., 2010). Thus, it seems rather unlikely that a very high Nd concentration accompanied with a very low Hf concentration is only the result of different scavenging behavior between both elements.

Further south at station S2, just north of the STF, the HREE are 40% lower while the LREE are between 60% and 84% lower, and Hf is at its minimum value of 0.04 pmol/kg. The REE pattern shifts from a flatter shale normalized shape at S1 to a steeper seawater-like pattern at S2 with LREEs relatively depleted compared to HREEs ($La_N/Yb_N = 0.5$) and a lower Ce/Ce^* of −0.53 (Fig. 4 and Table 2). Although not very pronounced, this pattern, together with the overall low abundance of the REEs suggest either a low contribution from the dissolution of terrigenous material or enhanced scavenging due to higher productivity at the STF, most likely a combination of both processes. Hegner et al. (2007) reported low aluminum (Al) and thorium (Th) concentrations in particles documenting very low terrigenous inputs to this area thus providing an explanation for the low dissolved REE concentrations. These authors also proposed that scavenging of Nd from seawater on the order of only 5–10% of the available dissolved load would be sufficient to yield the observed Nd concentrations adsorbed to the particles. However, the slightly lower La_N/Yb_N ratios from our study between 0.19 and 0.29 from the STF to the BDY compared to the ones from the Weddell Gyre (~0.29 to 0.38) may indicate more ample scavenging, since LREE are preferentially scavenged to biogenic particles (e.g. Elderfield and Greaves, 1982). The low dissolved Nd concentrations in our surface water samples from the ACC can thus be explained by limited supply but additional scavenging also seems to be involved.

4.1.2. Antarctica and South America

The elemental distribution of the sampled stations near the Antarctic continent does not indicate strong terrigenous supply. Within the entire Weddell Gyre Hf and REE concentrations are elevated relative to the ACC but with no significant increases similar to those observed for S1 close to the Antarctic continent (Figs. 3 and 4). However, at stations S7 and 222, close to the volcanic King George Island (KGI, Fig. 2C) and east of the Antarctic Peninsula (AAP), respectively, the Hf and REE concentrations are clearly elevated. In particular, at S7 the Hf concentration of 0.38 pmol/kg is almost twice as high as it is on average in the Weddell Gyre, whereas the REE concentrations are on average only about 10–50% higher. At station 222 no significant increase of the Hf concentration in the surface water is observed. The more radiogtenic Hf and Nd isotope compositions at S7 ($\varepsilon_{Hf} = +6.1$ and of $\varepsilon_{Nd} = -4.0$,

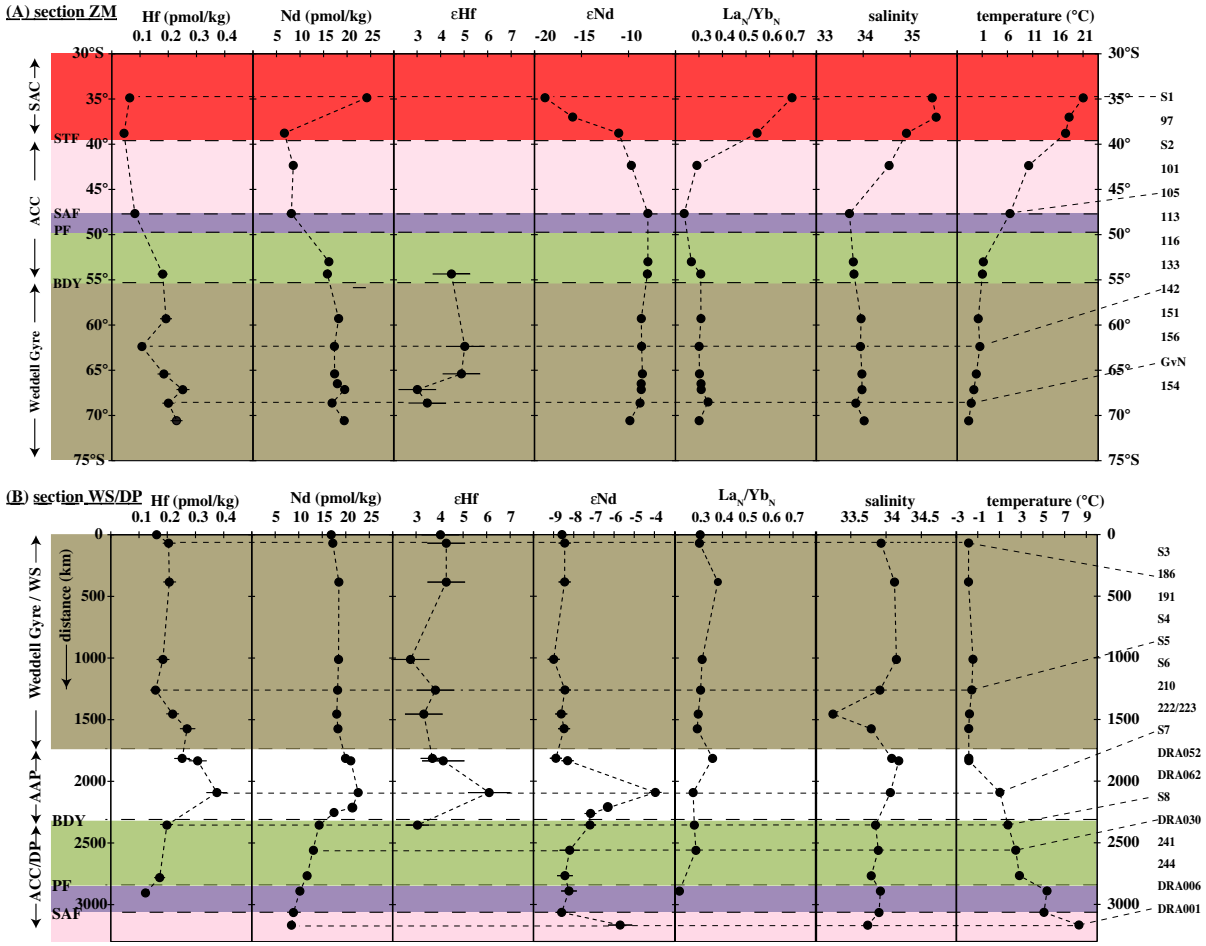

Fig. 3. Geochemical composition of the surface samples (<100 m water depth) along the Zero Meridian (A) and through the Weddell Sea and the Drake Passage (B), note the different scales in ε_{Nd} and temperature between (A) and (B). Major hydrographic transitions are marked by horizontal dashed lines (see text). Hafnium and Nd concentrations largely follow a similar pattern in both sections with the exception that S1 in (A) shows a significantly elevated Nd concentration. The Hafnium and Nd isotope compositions also follow similar trends where combined data are available. The only exceptions are stations 156 and GvN, where the ε_{Hf} drops to less radiogenic values, whereas ε_{Nd} does not. The La/Yb ratios are normalized to PAAS (Taylor and McLennan, 1985). Horizontal bars indicate the analytical uncertainties, which in most cases are smaller than symbol size.

respectively) clearly document external inputs of these elements from the basaltic rocks of KGI. The observed radiogenic Nd isotope composition accompanied only by a small increase of the REE concentrations implies a boundary exchange process with the KGI. A similar, though not as pronounced exchange of Nd isotopes has obviously influenced station 154, which has been sampled in 135 m water depth close to the seafloor at the Antarctic ice shelf. Here the Nd isotope composition of $\varepsilon_{Nd} = -9.9$ is more than 1 ε-unit lower than those in the nearby surface stations (Fig. 3B). A simple mass balance calculation, using the Nd isotope composition of station 154 ($\varepsilon_{Nd} = -9.9$), the average isotope composition of the Weddell Sea and that of glaciomarine sediments ($\varepsilon_{Nd} = -8.6$ and -15.0, respectively, this study; Roy et al., 2007; Stichel et al., 2012), suggests that about 20% of the Nd must be derived from shelf sediments off Dronning Maud Land. However, the increase of the Nd concentration and most of the REEs is less than 10% compared to the average surface concentration of 17.9 pmol/kg. In order to test if processes other than particle or sediment release are involved, we simply calculate a hypothetical ε_{Nd} signature only caused by exchange with particles based on the above considerations and compare it with the measured value. This is an approach similar to the one of Lacan and Jeandel (2001) using the following equation: $\varepsilon_{Nd\text{-}calc} = ([Nd]_{initial} * \varepsilon_{Nd\text{-}initial} + \Delta[Nd] * \varepsilon_{Nd\text{-}SED})/[Nd]_{meas}$, where $[Nd]_{initial}$ is the average concentration of surface waters in the Weddell Sea (18 pmol/kg), $[Nd]_{meas}$ the one of station 154 (19.4 pmol/kg), $\Delta[Nd]$ the difference in concentration (1.4 pmol/kg) and $\varepsilon_{Nd\text{-}initial}$ is the average isotope composition of the Weddell Sea surface waters ($\varepsilon_{Nd} = -8.6$). The isotope composition of the sediment ($\varepsilon_{Nd\text{-}SED} = -15.0$) is taken from Roy et al. (2007) close to station 154 of our study. If the calculated value is the same as the one observed, the difference in the isotope composition between these waters seems to be derived entirely by particle or sediment release. The calculated isotope composition of $\varepsilon_{Nd} = -9.1$, however, is about 0.8 ε_{Nd} units more radiogenic, which is just about higher than the external reproducibility of ± 0.4, but still suggests that boundary

exchange processes do influence the isotope composition at this location. If particle dissolution was the only process to explain the isotope composition at station 154, the corresponding Δ[Nd] must be ~4.5 pmol/kg, whereas the observed Δ[Nd] is only 1.4 pmol/kg.

The only significant drop towards less radiogenic Hf isotope compositions is observed at station 151 ($\varepsilon_{Hf} = +4.9$) and stations 156 and GvN nearest to Dronning Maud Land ($\varepsilon_{Hf} = +3.0$ and $\varepsilon_{Hf} = +3.4$, respectively; Fig. 3A). The proximity of these stations to the Antarctic shelf suggests an unradiogenic Hf input from the Dronning Maud Land (e.g. van de Flierdt et al., 2006, 2007). Although a shift to unradiogenic Nd is not observed for these stations the unradiogenic Nd isotope composition at the southernmost station 154 ($\varepsilon_{Nd} = -9.9$, ε_{Hf} is not available) also suggests Nd inputs from the Dronning Maud Land. In general, Nd isotopes in the WG are slightly less radiogenic than in the ACC (Table 1), also pointing at some Nd fluxes from Antarctica to the Weddell Sea. The less radiogenic Hf signatures observed in the vicinity of Dronning Maud Land may be a consequence of a relatively congruent release of Hf from the exposed rocks on land due to the glacial grinding of weathering resistant zircons. Evidence for a more congruent release of Hf under physical weathering conditions has previously been found in ferromanganese crusts, which recorded less radiogenic Hf isotope compositions than those of the seawater array in regions and during periods of prevailing enhanced physical weathering (Piotrowski et al., 2000; van de Flierdt et al., 2002, 2007). These authors concluded that the onset of Northern Hemisphere Glaciation and the accompanying enhanced physical weathering led to a more congruent release of Hf isotopes from the old continental crust in northern Canada and Greenland. However, the shift of the Hf isotope compositions in these studies was several ε_{Hf} units compared to only 1 ε_{Hf} unit in our case. Our data from the Weddell Sea in the proximity of Dronning Maud Land thus suggest that the local Hf isotope composition in this case is not a sensitive tracer for physical weathering inputs. Furthermore, the combined Hf and Nd isotope data do not plot significantly closer to the terrestrial array (Fig. 1).

The exchange with Antarctica is clearly more prominent at station S7, close to King George Island (KGI). Like most of the South Sandwich Islands, KGI is composed of relatively young, mafic island arc rocks (see Section 1.2). Previous studies on James Ross Island, which has the same geological origin as KGI (e.g. Machado et al., 2005) reported Hf and Nd isotope compositions of the bulk rocks of $\varepsilon_{Hf} \sim +7$ (Sims et al., 2008) and $\varepsilon_{Nd} \sim +5$ (Hole et al., 1994; Kosler et al., 2009). Enhanced weathering input from these rocks is also indicated by the high particulate concentrations of Hf and Nd (Hegner et al., 2007; Table 3), which are likely to modify the isotope composition of the surface waters. We thus also calculated the hypothetical Nd isotope composition only controlled by partial dissolution of particles at station S7, analogous to the approach above. We used the Nd isotope composition and concentration of station 230/50 m ($\varepsilon_{Nd} = -8.2$; 18.9 pmol/kg) as a representative value of surface waters from the Drake Passage. The isotope composition of KGI ranges from $\varepsilon_{Nd} = +1$ to +5 (Hole et al., 1994; Kosler et al., 2009), from which a hypothetical Nd isotope composition of $\varepsilon_{Nd} = -6.7$ to −6.0 is calculated. This is 2–2.7 ε_{Nd} units less radiogenic than the observed signatures (Fig. 3B). The observed Nd isotope composition of $\varepsilon_{Nd} = -4.0$ is therefore largely a result of boundary exchange rather than dissolution of weathered volcanic material. The REE pattern of S7 is similar to that of LCDW (Hathorne et al., 2012) and also suggests that elemental input derived from volcanic material (REE values from Machado et al., 2005) is of minor importance (Fig. 4).

The observed radiogenic Hf isotope composition at KGI of $\varepsilon_{Hf} = +6.1$ (S7) also indicates a significant influence from weathering inputs on the surface water isotope composition. The Hf concentration of 0.38 pmol/kg is also significantly higher than the average in the Weddell Sea or the ACC (Fig. 3 and Table 1). Applying the same approach as for Nd reveals that the hypothetical Hf isotope composition should be between +3.8 and +5.4, using average compositions of the Weddell Gyre and the ACC ($\varepsilon_{Hf\text{-initial}} = +3$ to +4 and $[Hf]_{initial} = 0.2$ to 0.3 pmol/kg). The observed Hf isotope composition at S7, however, is $\varepsilon_{Hf} = +6.1$, indicating again that boundary exchange processes govern the isotope composition rather than addition of dissolved Hf from particles or weathered material.

The peak radiogenic Hf and Nd isotope values sharply decrease towards less radiogenic levels of $\varepsilon_{Nd} = -6.3$ (DRA052) and $\varepsilon_{Nd} = -7.2$; $\varepsilon_{Hf} = +3$ (S8 and DRA062) towards the Drake Passage, implying that the influence of KGI is locally limited and that the boundary exchange signals are rapidly diluted by surface ocean waters from the Drake Passage. The imprint on the Hf isotope compositions is even more locally confined and is only detected at station 7. This is explained by the lower isotopic contrast for Hf between station 7 ($\varepsilon_{Hf} = +6.1$) and the "typical" ACC surface ocean ($\varepsilon_{Hf} \sim +4$, Fig. 3B) relative to the contrast observed for Nd isotopes, but may also reflect a shorter surface ocean residence time for Hf than for Nd as suggested before (Rickli et al., 2010). A more radiogenic Nd isotope signal is again observed in the northern part of the Drake Passage (Fig. 3B). At station DRA001 the Nd isotope composition of $\varepsilon_{Nd} = -5.7$ implies radiogenic input from the southern tip of South America, possibly derived from the Pali Aike Volcanic Field, which consist of lavas with a Nd isotope composition as radiogenic as $\varepsilon_{Nd} \sim +5$ (D'Orazio et al., 2000). The imprint is only observed close to the coast and the Nd isotope composition of the open Drake Passage is indistinguishable from the ACC ε_{Nd} signatures of ~−8 along the Zero Meridian.

4.2. Cycling of Hf and Nd in the Southern Ocean

Previous studies have suggested that Hf and REEs are prone to scavenging by biogenic opal in the Southern Ocean (e.g. Rickli et al., 2009; Stichel et al., 2012). It was suggested that the large specific surface area of diatom frustules acts as an effective scavenger for Hf and Nd. Stichel et al. (2012) found that Hf and Nd concentrations correlate well with dissolved Si content in the Southern Ocean and suggested that the observed linear increase of Nd concentration with water depth represents a steady release of

Nd, while the frustules dissolve. This feature was not observed for Hf, indicating a different remineralization behavior. A comparison of particulate Nd/Hf ratios from our study with the particulate opal content in the eastern Atlantic sector of the ACC indicates a strong negative correlation between these parameters (Nd and opal data from Hegner et al. (2007); Fig. 5 and Table 3). This suggests that Hf is more efficiently scavenged from surface waters than Nd when siliceous frustules of diatoms are present. This means that diatom productivity acts as a more effective sink for Hf than for Nd in the Southern Ocean given that a significant fraction of the opal is buried in the sediment. However, one would expect that such an effect would influence the dissolved fraction as well, which is not observed (Fig. 5B). Except for stations S1, S2 and 142 the elemental distribution of Hf and Nd is very similar and does not support any fractionation by scavenging. One plausible explanation is that the particulate and dissolved fractions were collected separately on different expeditions. The particulate samples were taken between November 1997 and March 1998 (Hegner et al., 2007), whereas the dissolved fraction was sampled from February to April 2008. To estimate if and to what extent the diatoms contribute to a preferential scavenging or elemental fractionation, parallel collection of the particulate and dissolved fractions is required in future studies.

South of the ACC the dissolved concentrations for both elements are elevated and rather homogenous, with the exception of station 142, where the Hf concentration amounts to only 0.11 pmol/kg, i.e. only half of the average Hf concentration observed for other samples in this area. Hegner et al. (2007) also observed higher particulate Nd concentrations in the WG (more than 2 pmol/L) together with unradiogenic detrital Nd isotope compositions and high Al concentrations of up to 7.2 nmol/L, supporting supply of terrigenous material by icebergs. However, the elevated concentrations of Nd (~18 pmol/kg) and Hf (~0.21 pmol/kg) observed within the Weddell Gyre in our study compared to those north of the PF are more likely caused by accumulation of deep sourced Hf and Nd rather than derived from icebergs, as discussed below. The highest dissolved Hf and Nd concentrations south of the STF of 0.38 pmol/kg and 22.1 pmol/kg, respectively, were measured near the volcanic King George Island. This matches the highest concentrations in particulate Hf and Nd (2.88 pmol/L and 24.44 pmol/L, respectively, Hegner et al., 2007; Table 3), implying a strong input from this or adjacent islands.

Terrigenous influence is further supported by the isotope composition of particles in the Weddell Gyre yielding values $\varepsilon_{Nd} = -15$ or lower, suggesting an enhanced input of material from East Antarctica via ice rafting (Hegner et al., 2007). Alternatively, the Weddell Gyre's average dissolved Nd and Hf isotope composition is nearly identical to that of CDW ($\varepsilon_{Nd} = -8.5 \pm 0.3$, $\varepsilon_{Hf} = +4.4 \pm 0.6$, Stichel et al., 2012) in the studied area. This similarity may suggest that the isotope compositions of surface waters are the result of vigorous mixing and accumulation of these elements within the WG rather than reflecting the result of low terrigenous input. A supply of Hf and Nd from deeper waters is supported by relatively high surface water concentrations of ~0.2 pmol/kg and ~18 pmol/kg, respectively. Additionally, the REE patterns in the Weddell Gyre are very similar to the pattern of LCDW in Hathorne et al. (2012). On the basis of the distribution of the highly particle reactive elements Th and protactinium (Pa) in the Weddell Gyre, Rutgers van

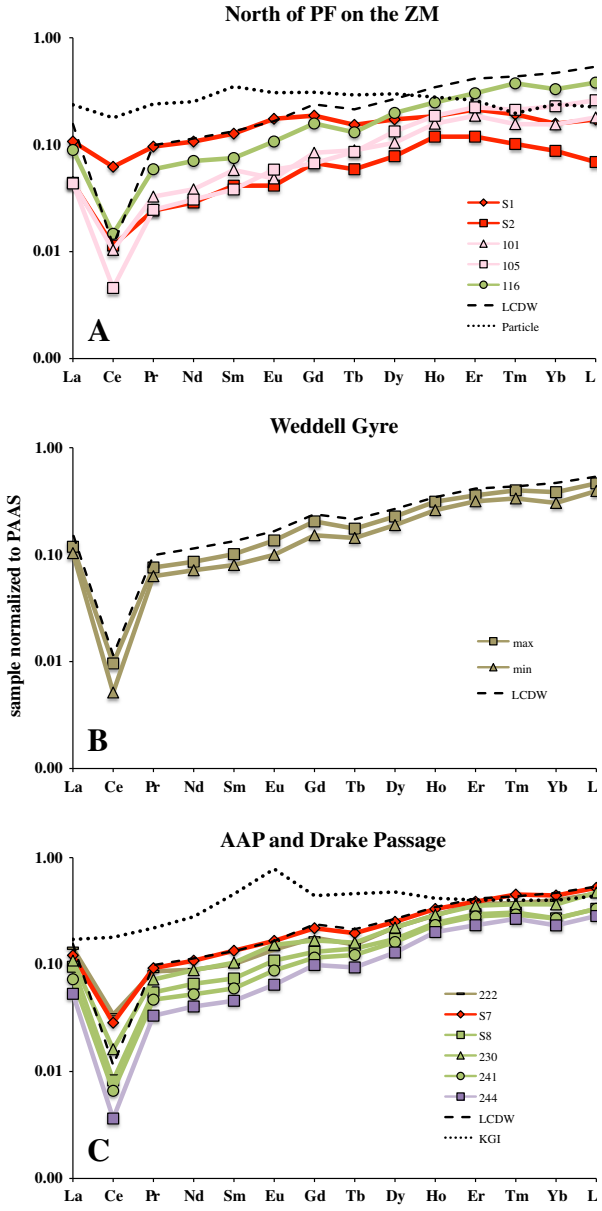

Fig. 4. Shalenormalized REE patterns of surface samples (<100 m depth) from north of the Polar Front on the Zero Meridian (A), the Weddell Gyre (B) and the Antarctic Peninsular including the Drake Passage (C). The color-coding corresponds to the zones illustrated in Fig. 3. Additional patterns are shown for comparison: The composition of suspended particles close to South Africa (A, Hegner et al., 2007), Lower Circumpolar Deep Water (LCDW) at 2000 m in the Weddell Gyre (A–C, Hathorne et al., 2012) and the composition of volcanic rocks of King George Island (C, Machado et al., 2005). Seawater values are normalized to PAAS multiplied by 10^6, whereas the normalized particulate values are multiplied by 0.01 to fit on the same scale.

der Loeff and Berger (1993) documented that particle export and thus scavenging is very low leading to their accumulation in the water column of the Weddell Gyre. The general homogeneity of Hf and REE within the Weddell Gyre also suggests accumulation of these elements. This observation can be used to estimate the minimum residence time of Hf and REE in surface waters within the Weddell Gyre. The average residence time of a parcel of surface water there is around 2.5 years (Gordon and Huber, 1990; Hoppema et al., 1995), implying that the residence times of Hf and the REEs is at least in that order.

5. SUMMARY AND CONCLUSIONS

In this study the first combined surface water Hf and Nd isotope compositions and Hf and REE concentrations of surface waters from the Atlantic sector of the Southern Ocean are presented. The data set comprises a wide range of Hf and Nd concentrations from low values in the South Atlantic Current (0.04 and 6.7 pmol/kg) to maximum values near King George Island (0.38 and 22.6 pmol/kg).

(1) The highest Nd concentrations were found in surface waters southwest of Cape Town. In the same sample, a very low Hf concentration indicates restricted release of Hf from the South African continental crust. High La_N/Yb_N ratios between 0.50 and 0.68 and markedly flat PAAS-normalized REE patterns support enhanced terrigenous input from South Africa. This is accompanied by the least radiogenic Nd isotope composition as low as $\varepsilon_{Nd} = -18.9$, which was probably advected via the Agulhas Current and documents inputs from weathering of Archean cratonic rocks exposed in South Africa.

(2) The low elemental concentrations just north of the Subantarctic Front most likely result from a combination of limited terrigenous supply and high biological productivity. A good correlation of the particulate Nd/Hf ratio with biogenic SiO_2 content suggests a preferential scavenging of Hf onto siliceous frustules. The Hf and Nd concentrations are lower north of the PF and increase southward to more constant values within the WG indicating accumulation resulting from low biogenic particle fluxes and thus a weak scavenging efficiency of trace metals.

(3) We observe the influence of volcanic rocks by marked increases of Hf and Nd concentrations in the vicinity of King George Island. These are, accompanied by a pronounced excursion to more radiogenic isotope compositions for both elements ($\varepsilon_{Hf} = +6.1$; $\varepsilon_{Nd} = -4.0$). Mass balance considerations suggest that not only elemental release originating from particle dissolution but also boundary exchange processes govern the isotope composition of surface waters. A similar influence from mantle-derived rocks is observed at the southern tip of Chile. Boundary exchange processes most likely also take place on the Antarctic shelf where less radiogenic Nd than the average composition of the Weddell Gyre is found at 135 m water depth close to the seafloor.

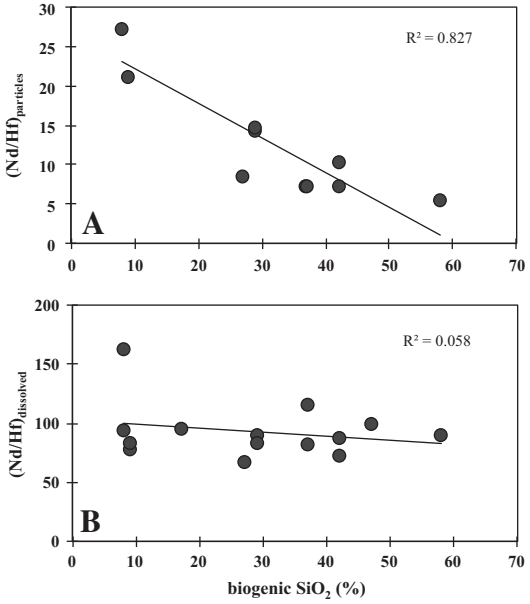

Fig. 5. Nd/Hf ratio in particles (A) and in the dissolved fraction (B) plotted against the biogenic opal content in particles (Hegner et al., 2007).

(4) The Hf and Nd isotope compositions of the surface samples are shifted towards more radiogenic Hf values for given Nd values when compared to the "terrestrial array" and plot on the "seawater array".

(5) The majority of the studied areas comprising the ACC and the Weddell Gyre shows essentially homogenous isotope compositions of $\varepsilon_{Hf} \sim +4$ and $\varepsilon_{Nd} \sim -8.5$, which is similar to the deep water compositions studied previously and documents strong vertical and lateral mixing of Hf and Nd south of the Polar Front, indicating a residence time at least as long as the turnover time of surface waters in the Weddell Gyre.

ACKNOWLEDGEMENTS

This study was funded by a Grant of the Deutsche Forschungsgemeinschaft (DFG) to M.F. (Project FR1198/2) within the priority program "Antarctic Research" (SPP 1158). We thank Jutta Heinze and Ana Kolevica for lab support and the chief scientists Eberhard Fahrbach and Hein de Baar, as well as Captain Stefan Schwarze and the crew of Polarstern for their contribution and bravery. Many thanks to Celia Venchiarutti for her help during sample collection and preparation. This manuscript was significantly improved by the comments and suggestions by editor Sidney Hemming and reviewers.

REFERENCES

Albarède F., Simonetti A., Vervoort J. D., Blichert-Toft J. and Abouchami W. (1998) A Hf-Nd isotopic correlation in ferromanganese nodules. *Geophys. Res. Lett.* **25**, 3895–3898.

Arsouze T., Dutay J.-C., Lacan F. and Jeandel C. (2009) Reconstructing the Nd oceanic cycle using a coupled dynamical – biogeochemical model. *Biogeosciences* **6**, 2829–2846.

Bau M. and Koschinsky A. (2006) Hafnium and neodymium isotopes in seawater and in ferromanganese crusts: the "element perspective". *Earth Planet. Sci. Lett.* **241**, 952–961.

Bayon G., Vigier N., Burton K. W., Jean Carignan A. B., Etoubleau J. and Chu N.-C. (2006) The control of weathering processes on riverine and seawater hafnium isotope ratios. *Geology* **34**, 433.

Bayon G., Burton K. W., Soulet G., Vigier N., Dennielou B., Etoubleau J., Ponzevera E., German C. R. and Nesbitt R. W. (2009) Hf and Nd isotopes in marine sediments: constraints on global silicate weathering. *Earth Planet. Sci. Lett.* **277**, 318–326.

Cole D. I. (1992) Evolution and development of the Karoo Basin. In *Inversion Tectonics of the Cape Fold Belt* (eds. M. J. de Wit and I. G. D. Ransome). Karoo and Cretaceous Basins of Southern Africa, Balkema, Rotterdam, pp. 87–100.

Chen T.-Y. et al. (2011) Zircon effect alone insufficient to generate seawater Nd-Hf isotope relationships. *Geochem. Geophys. Geosyst.* **12**, Q05003. http://dx.doi.org/10.1029/2010GC003363.

Dalziel I. W. D. (1992) Antarctica – a tale of 2 supercontinents. *Annu. Rev. Earth Planet. Sci.* **20**, 501–526.

David K., Frank M., O'Nions R. K., Belshaw N. S. and Arden J. W. (2001) The Hf isotope composition of global seawater and the evolution of Hf isotopes in the deep Pacific Ocean from Fe–Mn crusts. *Chem. Geol.* **178**, 23–42.

de Baar H. J. W., Bacon M. P. and Brewer P. G. (1983) Rare-earth distributions with a positive Ce anomaly in the Western North Atlantic Ocean. *Nature* **301**, 324–327.

de Baar H. J. W., Bacon M. P., Brewer P. G. and Bruland K. W. (1985) Rare earth elements in the Pacific and Atlantic. *Oceans* **49**, 1943–1959.

Deacon G. E. R. (1979) The Weddell gyre. *Deep Sea Res. Part A. Oceanogr. Res. Papers* **26**, 981–995.

D'Orazio M., Agostini S., Mazzarini F., Innocenti F., Manetti P., Haller M. J. and Lahsen A. (2000) The Pali Aike Volcanic Field, Patagonia: slab-window magmatism near the tip of South America. *Tectonophysics* **321**, 407–427.

Elderfield H. and Greaves M. J. (1982) The rare earth elements in seawater. *Nature* **296**, 214–219.

Elderfield H., Upstillgoddard R. and Sholkovitz E. (1990) The rare earth elements in rivers, estuaries, and coastal seas and their significance to the composition of ocean waters. *Geochim. Cosmochim. Acta* **54**, 971–991.

Emery W. J. (1977) Antarctic polar frontal zone from Australia to the Drake Passage. *J. Phys. Oceanogr.* **7**, 811–822.

Fitzsimons I. (2000) A review of tectonic events in the East Antarctic Shield and their implications for Gondwana and earlier supercontinents. *J. Afr. Earth Sci.* **31**, 3–23.

Frank M., Whiteley N., Kasten S., Hein J. R. and O'Nions K. (2002) North Atlantic Deep Water export to the Southern Ocean over the past 14 Myr: evidence from Nd and Pb isotopes in ferromanganese crusts. *Paleoceanography* **17**, 1022. http://dx.doi.org/10.1029/2000pa000606.

Franzese A. M., Hemming S., Goldstein S. and Anderson R. (2006) Reduced Agulhas Leakage during the Last Glacial Maximum inferred from an integrated provenance and flux study. *Earth Planet. Sci. Lett.* **250**, 72–88.

German C. R., Klinkhammer G. P., Edmond J. M., Mitra A. and Elderfield H. (1990) Hydrothermal scavenging of rare-earth elements in the ocean. *Nature* **345**, 516–518.

German C. R., Masuzawa T., Greaves M. J., Elderfield H. and Edmond J. M. (1995) Dissolved Rare-Earth Elements in the Southern-Ocean - Cerium Oxidation and the Influence of Hydrography. *Geochim. Cosmochim. Acta* **59**, 1551–1558.

Godfrey L. V., Field M. P. and Sherrell R. M. (2008) The estuarine distributions of Zr, Hf and Ag in the Hudson River, and the implications for their continental and anthropogenic sources to seawater. *Geochem. Geophys. Geosyst.* **9**, Q12007. http://dx.doi.org/10.1029/2008GC002123.

Godfrey L. V., Zimmermann B., Lee D. C., King R. L., Vervoort J. D., Sherrell R. M. and Halliday A. N. (2009) Hafnium and neodymium isotope variations in NE Atlantic seawater. *Geochem. Geophys. Geosyst.* **10**, Q08015. http://dx.doi.org/10.1029/2009GC002508.

Gordon A. L. and Huber B. A. (1990) Southern ocean winter mixed layer. *J. Geophys. Res.* **95**, 11655–11672.

Greaves M., Statham P. and Elderfield H. (1994) Rare earth element mobilization from marine atmospheric dust into seawater. *Mar. Chem.* **46**, 255–260.

Haley B. A., Klinkhammer G. P. and McManus J. (2004) Rare earth elements in pore waters of marine sediments. *Geochim. Cosmochim. Acta* **68**, 1265–1279.

Halliday N., Davidson P., Owen M. and Olivarez M. (1992) Metalliferous sediments and the scavenging residence time of Nd near hydrothermal vents. *Geophys. Res. Lett.* **19**, 761–764.

Hathorne E., Haley B. A., Stichel T., Grasse P., Zieringer M. and Frank M. (2012) Online preconcentration ICP-MS analysis of rare earth elements in seawater. *Geochem. Geophys. Geosyst.* **13**, Q01020. http://dx.doi.org/10.1029/2011GC003907.

Hegner E., Dauelsberg H. J., Rutgers van der Loeff M. M., Jeandel C. and de Baar H. J. W. (2007) Nd isotopic constraints on the origin of suspended particles in the Atlantic Sector of the Southern Ocean. *Geochem. Geophys. Geosyst.* **8**, Q10008. http://dx.doi.org/10.1029/2007GC001666.

Hofmann E. E. (1985) The large-scale horizontal structure of the Antarctic circumpolar current from FGGE drifters. *J. Geophys. Res.* **90**, 7087–7097.

Hole M. J., Saunders A. D., Rogers G. and Sykes M. A. (1994) The relationship between alkaline magmatism, lithospheric extension and slab window formation along continental destructive plate margins. *Spec. Publ. Geol. Soc. London* **81**, 265–285.

Hoppema M., Fahrbach E., Schrder M., Wisotzki A. and de Baar H. J. W. (1995) Winter-summer differences of carbon dioxide and oxygen in the Weddell Sea surface layer. *Mar. Chem.* **51**, 177–192.

Jacobsen S. B. and Wasserburg G. J. (1980) Sm–Nd isotopic evolution of chondrites. *Earth Planet. Sci. Lett.* **50**, 139–155.

Jeandel C., Bishop J. K. and Zindler A. (1995) Exchange of neodymium and its isotopes between seawater and small and large particles in the Sargasso Sea. *Geochim. Cosmochim. Acta* **59**, 535–547.

Jeandel C., Venchiarutti C., Bourquin M., Pradoux C., Lacan F., van Beek P. and Riotte J. (2011) Single column sequential extraction of Ra, Nd, Th, Pa and U from a natural sample. *Geostand. Geoanal. Res.* **1–9**. http://dx.doi.org/10.1111/j.1751-908X.2010.00087.x.

Klatt O., Fahrbach E., Hoppema M. and Rohardt G. (2005) The transport of the Weddell Gyre across the Prime Meridian. *Deep Sea Res. Part II: Topical Stud. Oceanogr.* **52**, 513–528.

Kosler J., Magna T., Mlcoch B., Mixa P., Nyvlt D. and Holub F. (2009) Combined Sr, Nd, Pb and Li isotope geochemistry of alkaline lavas from northern James Ross Island (Antarctic Peninsula) and implications for back-arc magma formation. *Chem. Geol.* **258**, 207–218.

Lacan F. and Jeandel C. (2001) Tracing Papua New Guinea imprint on the central Equatorial Pacific Ocean using neodymium isotopic compositions and Rare Earth Element patterns. *Earth Planet. Sci. Lett.* **186**, 497–512.

Lacan F. and Jeandel C. (2005) Neodymium isotopes as a new tool for quantifying exchange fluxes at the continent–ocean interface. *Earth Planet. Sci. Lett.* **232**, 245–257.

Machado A., Lima E. F., Chemale F., Morata D., Oteiza O., Almeida D. P. M., Figueiredo A. M. G., Alexandre F. M. and Urrutia J. L. (2005) Geochemistry constraints of Mesozoic–Cenozoic calc-alkaline magmatism in the South Shetland arc, Antarctica. *J. S. Am. Earth Sci.* **18**, 407–425.

Millar I. L. and Pankhurst R. J. (1987) Rb–Sr geochronology of the region between the Antarctic Peninsula and the Transantarctic Mountains: Haag Nunataks and Mesozoic granitoids. In *Gondwana Six: Structure, Tectonics, and Geophys* (ed. G. D. McKenzie). Monogr. Ser, AGU, Washington, DC, pp. 151–160.

Millar I. L., Willan R. C. R., Wareham C. D. and Boyce A. J. (2001) The role of crustal and mantle sources in the genesis of granitoids of the Antarctic Peninsula and adjacent crustal blocks. *J. Geol. Soc.* **158**, 855–867.

Münker C., Weyer S., Scherer E. and Mezger K. (2001) Separation of high field strength elements (Nb, Ta, Zr, Hf) and Lu from rock samples for MC-ICPMS measurements. *Geochem. Geophys. Geosyst.* **2**. http://dx.doi.org/10.1029/2001GC000183.

Nowell G. M., Kempton P. D., Noble S. R., Fitton J. G., Saunders A. D., Mahoney J. J. and Taylor R. N. (1998) High precision Hf isotope measurements of MORB and OIB by thermal ionisation mass spectrometry: insights into the depleted mantle. *Chem. Geol.* **149**, 211–233.

Nowlin, Jr., W. D. and Whitworth, III, T. (1977) Structure and transport of the Antarctic circumpolar current at Drake Passage from short-term measurements. *J. Phys. Oceanogr.* **7**, 788–802.

Orsi A. H., Whitworth T. and Nowlin W. D. (1995) On the meridional extent and fronts of the Antarctic Circumpolar Current. *Deep Sea Res. Part I: Oceanogr. Res. Papers* **42**, 641–673.

Pankhurst R. J. et al. (1998) The Chon Aike province of Patagonia and related rocks in West Antarctica: a silicic large igneous province. *J. Volcanol. Geoth. Res.* **81**, 113–136.

Patchett P. J., White W. M., Feldmann H., Kielinczuk S. and Hofmann A. W. (1984) Hafnium rare-earth element fractionation in the sedimentary system and crustal recycling into the earths mantle. *Earth Planet. Sci. Lett.* **69**, 365–378.

Peterson R. and Stramma L. (1991) Upper-level circulation in the South Atlantic Ocean. *Prog. Oceanogr.* **26**, 1–73.

Pettke T., Lee D., Halliday A. N. and Rea D. K. (2002) Radiogenic Hf isotopic compositions of continental eolian dust from Asia, its variability and its implications for seawater Hf. *Earth Planet. Sci. Lett.* **202**, 453–464.

Piepgras D. J. and Jacobsen S. B. (1992) The behavior of rare earth elements in seawater: precise determination of variations in the North Pacific water column. *Geochim. Cosmochim. Acta* **56**, 1851–1862.

Pin C. and Zalduegui J. F. S. (1997) Sequential separation of light rare-earth elements, thorium and uranium by miniaturized extraction chromatography: Application to isotopic analyses of silicate rocks. *Anal. Chim. Acta* **339**, 79–89.

Piotrowski A. M., Lee D.-C., Christensen J. N., Burton K. W., Halliday A. N., Hein J. R. and Gunther D. (2000) Changes in erosion and ocean circulation recorded in the Hf isotopic compositions of North Atlantic and Indian Ocean ferromanganese crusts. *Earth Planet. Sci. Lett.* **181**, 315–325.

Rempfer J., Stocker T. F., Joos F., Dutay J.-C. and Siddall M. (2011) Modelling Nd-isotopes with a coarse resolution ocean circulation model: Sensitivities to model parameters and source/sink distributions. *Geochim. Cosmochim. Acta* **75**, 5927–5950.

Rickli J., Frank M. and Halliday A. N. (2009) The hafnium–neodymium isotopic composition of Atlantic seawater. *Earth Planet. Sci. Lett.* **280**, 118–127.

Rickli J., Frank M., Baker A. R., Aciego S., de Souza G., Georg R. B. and Halliday A. N. (2010) Hafnium and neodymium isotopes in surface waters of the eastern Atlantic Ocean: implications for sources and inputs of trace metals to the ocean. *Geochim. Cosmochim. Acta* **74**, 540–557.

Rogers J. J. W., Unrug R. and Sultan M. (1994) Tectonic assembly of Gondwana. *J. Geodyn.* **19**, 1–34.

Roy M., van de Flierdt T., Hemming S. R. and Goldstein S. L. (2007) $^{40}Ar/^{39}Ar$ ages of hornblende grains and bulk Sm/Nd isotopes of circum-Antarctic glacio-marine sediments: Implications for sediment provenance in the southern ocean. *Chem. Geol.* **244**, 507–519.

Rutgers van der Loeff M. M. and Berger G. W. (1993) Scavenging of ^{230}Th and ^{231}Pa near the Antarctic polar front in the South Atlantic. *Deep-Sea Res.* **40**, 339–357.

Rutberg R. L., Goldstein S. L., Hemming S. R. and Anderson R. F. (2005) Sr isotope evidence for sources of terrigenous sediment in the southeast Atlantic Ocean: Is there increased available Fe for enhanced glacial productivity? *Paleoceanography* **20**, PA1018.

Ryan W. B. F. et al. (2009) Global multi-resolution topography synthesis. *Geochem. Geophys. Geosyst.* **10**, Q03014. http://dx.doi.org/10.1029/2008GC002332.

Siddall M., Khatiwala S., van de Flierdt T., Jones K., Goldstein S., Hemming S. and Anderson R. (2008) Towards explaining the Nd paradox using reversible scavenging in an ocean general circulation model. *Earth Planet. Sci. Lett.* **274**, 448–461.

Sievers A. and Emery J. (1978) Variability of the Antarctic Polar frontal zone in the Drake Passage?? Summer 1976–1977. *J. Geophys. Res.* **83**, 3010–3022.

Sievers H. A. and Nowlin W. D. (1984) The stratification and water masses at Drake Passage. *J. Geophys. Res. Oceans* **89**, 489–514.

Sims K., Blichert-Toft J., Kyle P., Pichat S., Gauthier P., Blusztajn J., Kelly P., Ball L. and Layne G. (2008) A Sr, Nd, Hf, and Pb isotope perspective on the genesis and long-term evolution of alkaline magmas from Erebus volcano, Antarctica. *J. Volcanol. Geoth. Res.* **177**, 606–618.

Stichel T., Frank M., Rickli J. and Haley B. (2012) The hafnium and neodymium isotope composition of the Atlantic sector of the Southern Ocean. *Earth Planet. Sci. Lett.* **317–318**, 282–294.

Storey B. C. (2005) Antarctic. In *Encyclopedia of Geology* (eds. R. C. Selley, L. R. M. Cocks and Ian R. Plimer). Elsevier, Oxford, pp. 132–140.

Stramma L. and Peterson R. G. (1990) The South Atlantic current. *J. Phys. Oceanogr.* **20**, 846–859.

Tachikawa K., Jeandel C. and Roy-Barman M. (1999) A new approach to the Nd residence time in the ocean: the role of atmospheric inputs. *Earth Planet. Sci. Lett.* **170**, 433–446.

Tanaka T., Togashi S., Kamioka H., Amakawa H., Kagami H., Hamamoto T., Yuhara M., Orihashi Y., Yoneda S., Shimizu H., Kunimaru T., Takahashi K., Yanagi T., Nakano T., Fujimaki H., Shinjo R., Asahara Y., Tanimizu M. and Dragusanu C. (2000) JNdi-1: a neodymium isotopic reference in consistency with LaJolla neodymium. *Chem. Geol.* **168**, 279–281.

Taylor S. R. and McLennan S. M. (1985) *The Continental Crust: Its Composition and Evolution*. Blackwell Scientific, Boston, Mass.

Thomas R. J., von Veh M. W. and McCourt S. (1993) The tectonic evolution of southern Africa: an overview. *J. Afr. Earth Sc.* **16**, 5–24.

van de Flierdt T., Frank M., Lee D.-C. and Halliday A. N. (2002) Glacial weathering and the hafnium isotope composition of seawater. *Earth Planet. Sci. Lett.* **201**, 639–647.

van de Flierdt T., Hemming S. R., Goldstein S. L. and Abouchami W. (2006) Radiogenic isotope fingerprint of Wilkes Land–

Adélie Coast Bottom Water in the circum-Antarctic Ocean. *Geophys. Res. Lett.* **33**, L12606. http://dx.doi.org/10.1029/2006GL026020.

van de Flierdt T., Goldstein S., Hemming S., Roy M., Frank M. and Halliday A. (2007) Global neodymium–hafnium isotope systematics — revisited. *Earth Planet. Sci. Lett.* **259**, 432–441.

van de Flierdt T. and Pahnke K.Geotraces intercalibration participants (2012) GEOTRACES intercalibration of neodymium isotopes and rare earth elements in seawater and marine particulates – Part 1: international intercomparison. *Limnol. Oceanogr. Methods* **10**, 234–251.

Vervoort J. D., Patchett P. J., Blichert-Toft J. and Albarède F. (1999) Relationships between Lu-Hf and Sm-Nd isotopic systems in the global sedimentary system. *Earth Planet. Sci. Lett.* **168**, 79–99.

White W., Patchett J. and BenOthman D. (1986) Hf isotope ratios of marine sediments and Mn nodules: evidence for a mantle source of Hf in seawater. *Earth Planet. Sci. Lett.* **79**, 46–54.

Whitworth, III, T. (1980) Zonation and geostrophic flow of the Antarctic circumpolar current at Drake Passage. *Deep Sea Res. Part A. Oceanogr. Res. Papers* **27**, 497–507.

Zimmermann B., Porcelli D., Frank M., Rickli J., Lee D. and Halliday A. (2009a) The hafnium isotope composition of Pacific Ocean water. *Geochim. Cosmochim. Acta* **73**, 91–101.

Zimmermann B., Porcelli D., Frank M., Andersson P. S., Baskaran M., Lee D.-C. and Halliday A. N. (2009b) Hafnium isotopes in Arctic Ocean water. *Geochim. Cosmochim. Acta* **73**, 3218–3233.

Associate editor: Sidney Hemming